Pergamon

Int. J. Solids Structures Vol. 31, No. 17, pp. 2347–2366, 1994

0020–7683/94 $7.00 + .00

0020–7683(94)E0025–Q

MODE INTERACTION ANALYSIS OF STIFFENED SHELLS USING "LOCALLY BUCKLED" ELEMENTS

SRINIVASAN SRIDHARAN and MADJID ZEGGANE
Department of Civil Engineering, Washington University in St. Louis, Missouri 63130, U.S.A.

and

JAMES H. STARNES, JR
NASA Langley Research Center, Hampton, Virginia 23665, U.S.A.

(*Received* 12 *October* 1993; *in revised form* 31 *January* 1994)

Abstract—A novel methodology for the analysis of local and overall instabilities in stiffened plates and shells is proposed. The method consists of embedding the local buckling deformation—the buckling mode together with the associated second order fields—in an appropriate shell element. The local buckling deformation is controlled by a relatively small number of degrees of freedom which also allow for amplitude modulation. Examples of stringer-stiffened plates and shells subjected to axial compression are presented. Excellent agreement is found to exist between the results given by the method and those obtained from full blown nonlinear analysis and experiments. It is shown that the proposed technique offers a simple and considerably less expensive approach to mode interaction problems than conventional nonlinear finite element analysis. Imperfection-sensitivity under coincident buckling of axially compressed stringer-stiffened cylindrical shells is explored and it is shown that there can be an erosion of 50% of the load carrying capacity under imperfections of the kind unavoidable in practice.

NOTATION

Only the most important symbols are identified below:

A	area of cross-section
$[A], [B], [D]$	laminate stiffness matrices
$[B_0], [B_1^s], [B_1^s]$	matrices relating strains to the degrees of freedom
E	Young's modulus of (isotropic) material
E_1, E_2	elastic constants in the fiber and transverse directions
G_{12}	inplane shear modulus
$[H]$	constitutive relationship matrix
L	length of the structure
L_1, L_2	linear and quadratic operators
P_L	local buckling load
P_E	Euler buckling load
R	radius of curvature
W_c	displacement at the center as given by the "overall" field
W_{max}	maximum normal (combined) displacement
b	width of the panel
h	thickness of the plate-shell
h_0	averaged thickness of the plate
d_s	depth of the stiffener
m	number of half-waves of local buckling
p	polynomial degree of the shape function
t	a parameter having the dimension of length
t_s	thickness of the stiffener
ε	vector of generic strain
λ	load parameter
λ_c	critical value of λ
ν_{12}	inplane Poisson ratio
$\bar{\xi}_1, \bar{\xi}_2$	initial overall and local imperfections divided by h_0, respectively
ξ_1^0, ξ_2^0	actual overall and local imperfections
ξ	maximum local buckling amplitude
σ	axial stress carried by the structure
$\boldsymbol{\sigma}$	vector of generic stress
$\boldsymbol{\sigma}^0$	prebuckling stress vector (uniform axial stress applied at the ends)
σ_1	overall critical stress
σ_2	local critical stress.

INTRODUCTION

General

Stiffened plates and shells constitute important types of engineered structures. They find extensive applications in aerospace structures, where they are often fabricated out of advanced composites. Because of the slenderness of the walls typically employed in these components, stability criteria dominate their design.

Under axial compression, unstiffened shells are notorious for their extreme imperfection-sensitivity. This sensitivity is the result of destabilizing nonlinear interaction of a large number of nearly coincident modes of buckling. However, a stringer-stiffened shell under axial compression is not nearly as imperfection-sensitive, as the stiffeners can effectively act as nodal lines, thus precluding most, if not all, of the modes which cause radial deflections along them.

Two distinctive modes of buckling dominate the behavior of the stiffened shells (Fig. 1): (i) the short-wave local mode(s) in which the stiffener–skin junction remains essentially straight, i.e. the shell-skin buckles between the stiffeners; (ii) the overall long-wave mode in which the cross-sections of the stiffeners undergo significant translations in the direction normal to the shell, i.e. shell-skin bends carrying the stiffeners with it.

Optimum design of the shells often leads to a configuration for which the critical stresses corresponding to these modes are close to each other. Such optimized configurations are often extremely imperfection-sensitive due to the nonlinear modal interaction of the principal modes of buckling. The work of Koiter and Pignataro (1976a, b) is perhaps the most significant in the field of modal interaction in axially compressed stiffened shells. They introduced the concept of amplitude modulation, which accounts for the slowly varying amplitude of local buckling in the axial direction. Their analysis was based on drastic simplification of the local buckling response and is applicable for structures simply supported at the ends. Byskov and Hutchinson (1977) analysed complete cylindrical shells using "smeared" modelling for overall buckling and Koiter's solution for local buckling. Amplitude modulation was not considered and a mixed second order field, which arises by the interaction of local and overall modes, was computed. However, the displacement functions chosen for this field appear to be restrictive if not arbitrary. Significant imperfection-sensitivity at near coincident critical stresses was noticed. It appears that the problem has received so far only a perfunctory treatment and several questions regarding the phenomenon and the degree of erosion of the load-carrying capacity that may occur as a result of modal interaction have not been resolved.

Despite the stupendous wealth of literature and the currently available power of computer hardware, the finite element analysis of interactive buckling in shells has not been attempted with any degree of seriousness, even though the problem is recognized to be one of considerable importance (Bushnell, 1985). This is because the solution to these problems requires the use of a sufficiently fine mesh to capture the local deformation (such as a sinusoidal ripple of small wave length) in a structure which must be long enough for the

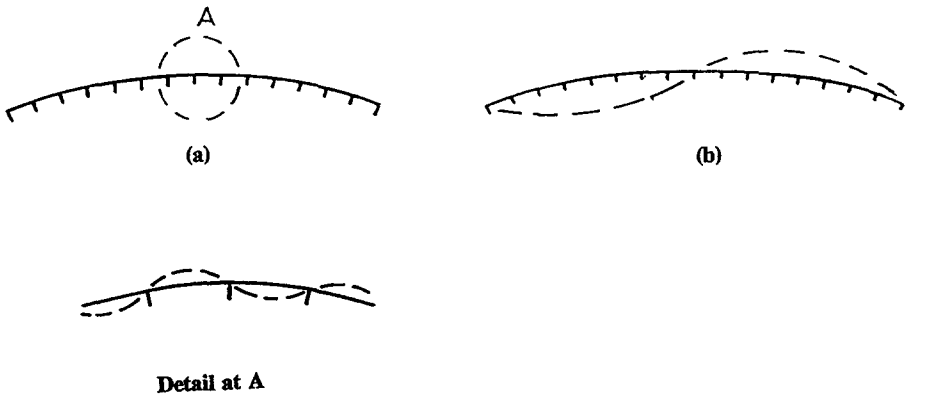

Fig. 1. Cross-section of a stiffened shell and the modes or buckling: (a) the local mode; (b) the overall mode.

overall instability to be of importance. As a result, phenomenal computational resources will be needed.

The concept of "locally buckled" elements

In this paper a novel concept which would greatly facilitate the analysis of modal interaction in shells is advanced. We note that local buckling occurs in a more or less periodic pattern in a structure having regular spacings of stiffeners. Thus, it is a relatively simple matter to compute *a priori* the local buckling mode and the associated postlocal buckling effects using a substructure of the shell. Once analysed, these deformations are embedded in an appropriate finite element with appropriate additional degrees of freedom which dictate their growth. As a result, the element, even if spanning several half-waves of local buckling, acquires the capability to depict the interaction without loss of accuracy as the loading proceeds. The element contains the vital local buckling information and readily manifests its effects under appropriate loading. Both local and overall imperfections can be readily accounted for. Though the concept appears to be wide in scope, the present treatment is restricted to stringer-stiffened shells primarily under axial compression.

The present approach also incorporates the concept of amplitude modulation. Sridharan and Peng (1989) showed that in stiffened plates the amplitude modulation performs the function of capturing the effects of several near coincident local modes of substantially the same transverse description but having slightly varying wavelengths in the axial direction. It is easy to show that the amplitude modulation performs a similar role in stiffened shells too and is therefore incorporated in the present analysis as well.

Typical examples of plate and shell panels are solved. Comparisons with solutions of the Tvergaard panel (Tvergaard, 1973) given by ABAQUS (1992), a well established commercial program, and the experimental results of Thompson *et al.* (1976), are made to verify the numerical model. The paper also discusses the evaluation of the mixed second order fields and their contribution to the modal interaction. It is shown that the modal interaction can, in stiffened shells, cause a significant erosion of the load-carrying capacity of the shell, of the order of 50% from the critical value, at such levels of imperfections as may be unavoidable in practice.

THEORY

In this section, the theoretical basis of the present finite element model is first outlined. This is followed by a description of the features of the shell element to be employed in the nonlinear analysis of the structure.

Displacement, strain and stress vectors

The essential displacement variables are given by:

$$\{\boldsymbol{u}\}^{\mathrm{T}} = \{u, v, w, \alpha, \beta\} \tag{1}$$

where u, v and w are the displacement components in the axial (x), transverse (y) and outward normal (z) directions, respectively at any point on the middle surface shell or stiffener (Fig. 2) and α and β are the rotations of the normal in the xz and yz planes, respectively.

The generic strain vector $\{\boldsymbol{\varepsilon}\}$ may now be defined as in the Reissner–Mindlin theory:

$$\{\boldsymbol{\varepsilon}\}^{\mathrm{T}} = \{\varepsilon_x, \varepsilon_y, \gamma_{xy}, \chi_x, \chi_y, \chi_{xy}, \gamma_{xz}, \gamma_{yz}\}. \tag{2}$$

Of these, $\{\bar{\boldsymbol{\varepsilon}}\} = \{\varepsilon_x, \varepsilon_y, \gamma_{xy}\}$ are the inplane strain components, $\{\boldsymbol{\chi}\} = \{\chi_x, \chi_y, \chi_{xy}\}$ are the curvature components, and $\{\boldsymbol{\gamma}\} = \{\gamma_{xz}, \gamma_{yz}\}$ are the transverse shearing strain components.

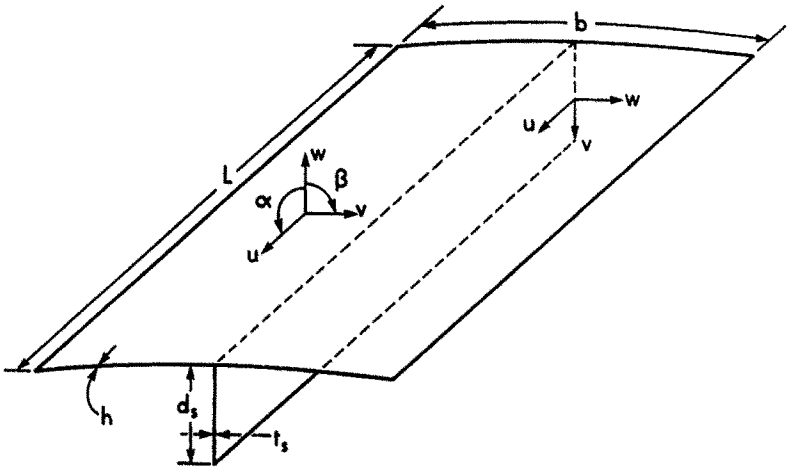

Fig. 2. Coordinate axes and dimensions of a stiffened panel.

The following strain–displacement relations are assumed for the shell/stiffener:

$$\varepsilon_x = \frac{\partial u}{\partial x} + \frac{1}{2}\left\{\left(\frac{\partial v}{\partial x}\right)^2 + \left(\frac{\partial w}{\partial x}\right)^2\right\}$$

$$\varepsilon_y = \frac{\partial v}{\partial y} + \frac{w}{R} + \frac{1}{2}\left\{\left(\frac{\partial u}{\partial y}\right)^2 + \left(\frac{\partial w}{\partial y}\right)^2\right\}$$

$$\gamma_{xy} = \frac{\partial u}{\partial y} + \frac{\partial v}{\partial x} + \frac{\partial w}{\partial x}\frac{\partial w}{\partial y}$$

$$\chi_x = \frac{\partial \alpha}{\partial x}$$

$$\chi_y = \frac{\partial \beta}{\partial y}$$

$$\chi_{xy} = \frac{\partial \alpha}{\partial y} + \frac{\partial \beta}{\partial x}$$

$$\gamma_{xz} = \alpha + \frac{\partial w}{\partial x}$$

$$\gamma_{yz} = \beta + \frac{\partial w}{\partial y}. \tag{3a–h}$$

These may be viewed as Donnell's strain–displacement relations modified to account for transverse shear deformation and the large inplane motions of stiffeners such as would occur under overall buckling. Thus the expression ε_x is augmented to include a nonlinear term in v, a key term which enables the modelling of overall bending/buckling phenomena. These equations may be expressed in the abbreviated form;

$$\varepsilon_i = L_{1_{ij}}(u_j) + \tfrac{1}{2}L_{2_{ij}}(u_j) \tag{4}$$

with $i = 1, \ldots, 8$ and $j = 1, \ldots, 5$.

To correspond with $\{\varepsilon\}$, a generic stress vector $\{\sigma\}$ is defined. This consists of force resultants $\{N\} = \{N_x, N_y, N_{xy}\}$, moment resultants $\{M\} = \{M_x, M_y, M_{xy}\}$ and transverse shear forces $\{Q\} = \{Q_x, Q_y\}$. The stress–strain relations are taken in the standard form (Sridharan *et al.*, 1992)

$$\begin{Bmatrix} N \\ M \end{Bmatrix} = \begin{bmatrix} A & B \\ B & D \end{bmatrix} \begin{Bmatrix} \bar{\varepsilon} \\ \chi \end{Bmatrix}$$

$$\{Q\} = k\bar{G}t\{\gamma\} \tag{5}$$

where $\bar{G}$ is the averaged transverse shear modulus, t is the thickness shell/stiffener, k is the shear correction factor (taken as 5/6). These equations may be written in the abbreviated form: $\sigma_i = H_{ij}\varepsilon_j$.

Determination of the local buckling fields

The linear stability (eigen-value) problem. The local buckling problem is solved following the standard finite strip procedure (Sridharan *et al.*, 1992). The salient features thereof will now be mentioned. The following notation will be employed in the sequel. A single superscript over a displacement, stress or strain will indicate a first order quantity and a double superscript will refer to a second order quantity; the superscript (1) is reserved for the overall buckling mode, while (2) and higher numbers will refer to the local modes considered in the ascending order of the corresponding critical stresses (note however, in this paper only a single local mode is considered); double superscripts (22) and (12) indicate the second order field associated with the local mode and a mixed second order field (m.s.o.f.), respectively.

The quadratic potential energy function governing the problem may, then, be written in the form

$$\Pi^{(2)} = \tfrac{1}{2}[H_{ij}L_{1_{ik}}(u_k^{(2)}) \cdot L_{1_{jl}}(u_l^{(2)}) + \sigma_i^0 \cdot L_{2_{ik}}(u_k^{(2)})] \tag{6}$$

where σ_i^0 represents the stress in the unbuckled state, and a dot operation indicates multiplication and integration over the volume of the structure (Budiansky, 1966).

For a stringer-stiffened cylindrical shell composed of a specially orthotropic material, the displacement functions that satisfy the differential equations are of the form

$$\{u^{(2)}, \alpha^{(2)}\} = \{u_i^{(2)}, \alpha_i^{(2)}\}\psi_i(y)\sin\left(\frac{m\pi x}{L}\right)$$

$$\{v^{(2)}, w^{(2)}, \beta^{(2)}\} = \{v_i^{(2)}, w_i^{(2)}, \beta_i^{(2)}\}\psi_i(y)\cos\left(\frac{m\pi x}{L}\right). \tag{7}$$

Here u_i, v_i, ... etc. are the degrees of freedom (d.o.f.) and ψ_i are appropriately chosen polynomial shape functions. In the present work, the functions ψ_i are chosen in a hierarchical form in the manner advocated by Szabo and Babuska (1991). These will be discussed later once again. For sufficiently large m, the boundary conditions at the end are deemed not to influence the local buckling process.

Designating the d.o.f.s of the local buckling problem as $q_i^{(2)}$, the potential energy function [eqn (6)] may be expressed in the form

$$\Pi^{(2)} = \tfrac{1}{2}\{a_{ij}^{(2)} - \lambda b_{ij}^{(2)}\}q_i^{(2)}q_j^{(2)} \tag{8}$$

where λ is the load parameter and i, j range over all the d.o.f.s considered in the buckling problem. The equilibrium equations follow:

$$\{a_{ij}^{(2)} - \lambda b_{ij}^{(2)}\}q_j^{(2)} = 0. \tag{9}$$

Solution of the linear eigen-value problem in eqn (9) gives the critical stress for local buckling and the eigen mode, $q_i^{(2)}$.

Second order field problem. The potential energy function governing the second order field problem is given by

$$\Pi^{(22)} = \tfrac{1}{2}[H_{ij}L_{1_{ik}}(u_k^{(22)})\cdot L_{1_{jl}}(u_l^{(22)}) + \sigma_i^0 \cdot L_{2_{ik}}(u_k^{(22)}) + H_{ij}\{L_{1_{ik}}(u_k^{(22)})\cdot L_{2_{jl}}(u_l^{(2)}) + 2L_{1_{ik}}(u_k^{(2)})\cdot L_{11_{jl}}(u_l^{(2)}, u_l^{(22)})\}] \quad (10)$$

where $\{\mathbf{u}^{(22)}\}$ refers to the second order field sought.

The displacement functions must be chosen keeping in view the solution to the differential equations of the second order field problem. The right hand side vector $\{\boldsymbol{r}\}$ of the differential equations consists of three sets of terms in general:

$$\{\boldsymbol{r}\} = \boldsymbol{r}^0(y) + \boldsymbol{r}^c(y)\cos\left(\frac{2m\pi x}{L}\right) + \boldsymbol{r}^s(y)\sin\left(\frac{2m\pi x}{L}\right). \quad (11)$$

The last two terms are rapidly varying trigonometric functions ($m \gg 1$) in x, while the first term is independent of x. The second order field problem may, then, be viewed as that of a cylindrical shell subjected to two loads which vary sinusoidally in the x-direction, together with a third term which remains constant in the x-direction. The solution takes the form

$$\{\boldsymbol{u}^{(22)}\} = \{\boldsymbol{u}^0\} + \{\boldsymbol{u}^c\}\cos\left(\frac{2m\pi x}{L}\right) + \{\boldsymbol{u}^s\}\sin\left(\frac{2m\pi x}{L}\right) \quad (12)$$

where $\{\boldsymbol{u}^0\}$ is a function of x and y, whereas $\{\boldsymbol{u}^c\}$ and $\{\boldsymbol{u}^s\}$ are functions of y only. Furthermore, $\{\boldsymbol{u}^0\}$ is a slowly varying function with respect to x. Note that the solution in the form of the buckling mode is ruled out because of the orthogonality condition, required by the asymptotic procedure (Budiansky, 1966). Also, because of the slowly varying nature of $\{\boldsymbol{u}^0\}$, it is decoupled in the solution process form $\{\boldsymbol{u}^c\}$ and $\{\boldsymbol{u}^s\}$.

Unlike in the asymptotic procedure for the initial postbuckling analysis (Sridharan *et al.*, 1992), it is not necessary to compute $\{\boldsymbol{u}^0\}$ at this stage. Rather we shall let it arise, by the interaction of $L_2(u_1)$ terms with the degree of freedom associated with the finite element mesh to be introduced later. Because of its slowly varying character, a relatively coarse finite element mesh must be able to pick up the deformation asociated with $\{\boldsymbol{u}^0\}$. So, we need to compute only the solution vectors associated with the trigonometric terms at this stage.

For a specially orthotropic material, the displacement fields to be computed take the simplified form:

$$\{u^{(22)}, \alpha^{(22)}\} = \{u_i^{(22)}, \alpha_i^{(22)}\}\psi_i(y)\sin\left(\frac{2m\pi x}{L}\right)$$

$$\{v^{(22)}, w^{(22)}, \beta^{(22)}\} = \{v_i^{(22)}, w_i^{(22)}, \beta_i^{(22)}\}\psi_i(y)\cos\left(\frac{2m\pi x}{L}\right) \quad (13)$$

where $u_i^{(22)}, \ldots$ etc. are the d.o.f.s second order field.

The potential energy function [eqn (10)] can now be expressed in terms of the d.o.f.s $q_r^{(2)}$ and $q_i^{(22)}$ defining the first and second order fields, respectively and takes the form

$$\Pi^{(22)} = \tfrac{1}{2}(a_{ij}^{(22)} - \lambda b_{ij}^{(22)})q_i^{(22)}q_j^{(22)} + c_{irs}q_i^{(22)}q_r^{(2)}q_s^{(2)} \quad (r,s = 1,\ldots,n_1); \quad (i,j = 1,2,\ldots,n_2) \quad (14)$$

where n_2 stands for the d.o.f.s of the trigonometric part of the second order field. The equation of equilibrium takes the form

$$(a_{ij}^{(22)} - \lambda b_{ij}^{(22)}) q_j^{(22)} = -c_{irs} q_r^{(2)} q_s^{(2)}, \tag{15}$$

λ is set equal to λ_{cr} in the calculations.

Amplitude modulation and mixed second order field

As a result of the interaction of local and overall modes, additional patterns of deformation are generated. To a first order of approximation, these are contained in the mixed second order field (m.s.o.f.). The governing differential equations of the field may be derived in the following manner. Let the total displacement be decomposed in the form

$$\{\boldsymbol{u}\} = \{\boldsymbol{u}^{(1)}\}\xi_1 + \{\boldsymbol{u}^{(2)}\}\xi_2 + \{\boldsymbol{u}^{(12)}\}\xi_1\xi_2 + \cdots \tag{16}$$

where ξ_1 and ξ_2 are the scaling factors associated with overall and local modes of buckling, respectively, and $\{\boldsymbol{u}^{(1)}\}$ represents the overall mode. The displacement associated with overall buckling would be significantly influenced by the end boundary conditions. Here, for the purposes of discussion, we assume that symmetry is available with respect to the center line of the cylindrical structure, so that the overall mode can be represented in the form:

$$\begin{aligned}
\boldsymbol{u}^{(1)} &= \sum_{n=1}^{N} u_n(y) \sin\left(\frac{n\pi x}{L}\right) \\
\boldsymbol{v}^{(1)} &= \sum_{n=0}^{N} v_n(y) \cos\left(\frac{n\pi x}{L}\right) \\
\boldsymbol{w}^{(1)} &= \sum_{n=0}^{N} w_n(y) \cos\left(\frac{n\pi x}{L}\right)
\end{aligned} \tag{17}$$

where N is expected to be small ($\ll m$) for a sufficiently accurate solution. Here we have assumed that it is possible to cast the overall buckling mode in the form given by eqn (17), using a finite strip formulation even in cases of end conditions other than simply supported. In the latter case, a single harmonic, namely $n = 1$, is sufficient.

Substituting the displacements in the form of eqn (16) in the governing nonlinear equations describing the buckled state of the shell, and equating coefficients of $\xi_1\xi_2$ on either side, we obtain the m.s.o.f. equations. We substitute for the overall buckling displacement, its nth harmonic contribution to obtain the corresponding component of the m.s.o.f. For simplicity, consider the classical Donnell type equations given in terms of the three displacement components u_{12}, v_{12} and w_{12}:

$$A_{11}\frac{\partial^2 u_{12}}{\partial x^2} + (A_{12} + A_{66})\frac{\partial^2 v_{12}}{\partial x\,\partial y} + A_{66}\frac{\partial^2 u_{12}}{\partial y^2}$$

$$= f_1(y)\cos\left(\frac{n\pi x}{L}\right)\sin\left(\frac{m\pi x}{L}\right) + g_1(y)\sin\left(\frac{n\pi x}{L}\right)\cos\left(\frac{m\pi x}{L}\right)$$

$$A_{22}\left(\frac{\partial^2 v_{12}}{\partial y^2} + \frac{\partial w_{12}}{R\,\partial y}\right) + (A_{12} + A_{66})\frac{\partial^2 u_{12}}{\partial x\,\partial y} + A_{66}\frac{\partial^2 v_{12}}{\partial x^2}$$

$$= f_2(y)\cos\left(\frac{n\pi x}{L}\right)\cos\left(\frac{m\pi x}{L}\right) + g_2(y)\sin\left(\frac{n\pi x}{L}\right)\sin\left(\frac{m\pi x}{L}\right)$$

$$D_{11}\frac{\partial^4 w_{12}}{\partial x^4} + 2(D_{12} + 2D_{66})\frac{\partial^4 w_{12}}{\partial x^2\,\partial y^2} + D_{22}\frac{\partial^4 w_{12}}{\partial y^4} + N_x^0\frac{\partial^2 w_{12}}{\partial x^2}$$

$$= f_3(y)\cos\left(\frac{n\pi x}{L}\right)\cos\left(\frac{m\pi x}{L}\right)+g_3(y)\sin\left(\frac{n\pi x}{L}\right)\sin\left(\frac{m\pi x}{L}\right). \quad (18a\text{–}c)$$

Note that f and g are functions of y, obtainable from the transverse variations of the local and overall modes.

The solution to this set of equations satisfying the boundary conditions yields the m.s.o.f. Also, the solution must satisfy an orthogonality condition with respect to the participating modes of buckling, which ensures that the higher order field is truly a "modification" of the deformation given by the modes of buckling.

The left hand side of eqns (18a–c) is governed by a linear stability operator and the right hand side represents two sinusoidally varying loading terms. Because of the rapidly varying nature of the trigonometric functions, the response is "local" in character and the use of von Karman kinematic relations employed in these equations is justified. The solution can be expressed in the form of the following sub-fields:

sub-field 1.

$$u_{12} = \bar{u}_{12}(y)\sin\left(\frac{m\pi x}{L}\right)\cos\left(\frac{n\pi x}{L}\right)$$

$$v_{12} = \bar{v}_{12}(y)\cos\left(\frac{m\pi x}{L}\right)\cos\left(\frac{n\pi x}{L}\right)$$

$$w_{12} = \bar{w}_{12}(y)\cos\left(\frac{m\pi x}{L}\right)\cos\left(\frac{n\pi x}{L}\right); \quad (19a\text{–}c)$$

sub-field 2.

$$u_{12} = u^*_{12}(y)\cos\left(\frac{m\pi x}{L}\right)\sin\left(\frac{n\pi x}{L}\right)$$

$$v_{12} = v^*_{12}(y)\sin\left(\frac{m\pi x}{L}\right)\sin\left(\frac{n\pi x}{L}\right)$$

$$w_{12} = w^*_{12}(y)\sin\left(\frac{m\pi x}{L}\right)\sin\left(\frac{n\pi x}{L}\right). \quad (20a\text{–}c)$$

Each of these fields takes the form of a local mode modulated by a slowly varying function. The most destabilizing contents of this field are the local modes whose eigen-values (critical stresses) are close to the fundamental local mode. In particular $\bar{w}_{12}(y)$ and $w^*_{12}(y)$ often contain a component identical to $\bar{w}(y)$, the transverse variation of the local mode. Thus, a consequence of the interaction is the "amplitude modulation" of the local mode.

Now, m.s.o.f. (the sub-fields taken together) may also be written in the following form:

$$u_{12} = \tfrac{1}{2}(\bar{u}_{12}+u^*_{12})\sin\left(\frac{(m+n)\pi x}{L}\right)+\tfrac{1}{2}(\bar{u}_{12}-u^*_{12})\sin\left(\frac{(m-n)\pi x}{L}\right)$$

$$v_{12} = \tfrac{1}{2}(\bar{v}_{12}+v^*_{12})\cos\left(\frac{(m+n)\pi x}{L}\right)+\tfrac{1}{2}(\bar{v}_{12}-v^*_{12})\cos\left(\frac{(m-n)\pi x}{L}\right)$$

$$w_{12} = \tfrac{1}{2}(\bar{w}_{12}+w^*_{12})\cos\left(\frac{(m+n)\pi x}{L}\right)+\tfrac{1}{2}(\bar{w}_{12}-w^*_{12})\cos\left(\frac{(m-n)\pi x}{L}\right). \quad (21)$$

In this form it is readily seen that the m.s.o.f. is orthogonal to the fundamental local mode. These two parts of the solution associated with wave numbers $m+n$ and $m-n$ are uncoupled

from each other and can be obtained using a finite strip formulation rendering the following potential energy function stationary:

$$\Pi^{(12)} = \tfrac{1}{2}[H_{ij}\{L_{1_{ik}}(u_k^{(12)})\cdot L_{1_{jl}}(u_l^{(12)}) + 2[L_{1_{ik}}(u_k^{(12)})\cdot L_{11_j}(u_l^{(1)}, u_l^{(2)}) + L_{1_{ik}}(u_k^{(1)})\cdot L_{11_j}(u_l^{(2)}, u_l^{(12)}) + L_{1_{ik}}(u_k^{(2)})\cdot L_{11_j}(u_l^{(1)}, u_l^{(12)})]\} + \sigma_i^0\cdot\{L_{2_{ik}}(u_k^{12}) + 2L_{11_j}(u_k^{11}, u_k^{22})\}]. \quad (22)$$

But the occurrence of the m.s.o.f. in the form of local modes [eqn (21)] can be a pitfall for an unsophisticated analyst. Because $m \gg n$, the eigen-values of the local modes with half-waves $m+n$ and $m-n$ are close to those of the primary local mode with half-wave number m. As $\lambda \to \lambda_{cr}$, the evaluation of the field is riddled by the singularity of the governing linear stability equations, leading to unacceptably poor results. The same is true for the contributions to m.s.o.f. associated with any $n \ll m$.

In order to eliminate the influence of the singularities, we employ here a local buckling field modulated by an as yet unknown modulating function, $F(x)$, at the very inception of the analysis. The adoption of the amplitude modulated local mode is equivalent to taking into account a number of local modes, all having the same transverse description, but of slightly differing wavelengths. This can be seen by expanding the modulating function $F(x)$ in the form of a Fourier series

$$F(x) = \sum_{n=0}^{N} a_n \cos\left(\frac{n\pi x}{L}\right) \quad (23)$$

so that,

$$\begin{aligned} w^{(2)} &= F(x)\bar{w}(y)\cos\left(\frac{m\pi x}{L}\right) \\ &= \bar{w}(y)\sum_{n=0}^{N} a_n \cos\left(\frac{n\pi x}{L}\right)\cos\left(\frac{m\pi x}{L}\right) \\ &= \tfrac{1}{2}\bar{w}(y)\sum_{n=0}^{N} a_n\left[\cos\left(\frac{(m+n)\pi x}{L}\right) + \cos\left(\frac{(m-n)\pi x}{L}\right)\right]. \end{aligned} \quad (24)$$

The adoption of the amplitude modulated local mode significantly alters the process of evaluation and the outcome of m.s.o.f. or any part thereof. But here we restrict our attention to the m.s.o.f. arising from the interaction of the primary local mode (which is the essential ingredient of the amplitude modulated local mode adopted here) and the nth harmonic component of the overall mode, the forms of which are given by eqn (21). These must now be rendered orthogonal to the local modes with wave numbers $m-n$, $m+n$ ($n = 1, 2, \ldots$). This can be achieved only by imposing orthogonality conditions between the transverse variation of $w^{(2)}$ on the one hand $\bar{w}_{12}$ and w_{12}^* on the other. Thus,

$$\begin{aligned} \int_A N_x^0 \bar{w}(y)\bar{w}_{12}(y)\,dA &= 0 \\ \int_A N_x^0 \bar{w}(y)w_{12}^*(y)\,dA &= 0 \end{aligned} \quad (25)$$

where N_x^0 is the axial force per unit length applied at the ends of the structure.

Each of these fields is evaluated by rendering the potential function [eqn (22)] stationary and simultaneously imposing the orthogonality condition via the Lagrangian multiplier technique. The solution must be repeated as n is varied and the contributions of all harmonics summed up. However N is expected to be a small number. Thus, the local

modes neighboring the fundamental local mode (which are accounted for by amplitude modulation) are eliminated from the m.s.o.f.

It sometimes happens that a secondary local mode, with a different transverse description, say $\bar{w}(y)$, is triggered in the process of interaction. This would be the result of certain components of the "loading term" on the r.h.s. of the m.s.o.f. equations being in sympathy with the secondary mode and the proximity of the eigen-value of the latter to that of the primary local mode. The doubly symmetric cross-sections are a case in point (Ashraf Ali and Sridharan, 1988). An examination of the normal displacement variation of the m.s.o.f. will reveal if this is indeed the case. In this event, in the interests of accuracy, the triggered mode must be named as an additional primary local mode and associated with yet another amplitude modulating function. The transverse variations of the m.s.o.f. must then be orthogonalized with respect to both $\bar{w}(y)$ and $\tilde{w}(y)$. With the local modes of buckling liable to be triggered removed from its arsenal, m.s.o.f. ceases to play a significant role in the analysis and will be neglected henceforth. A discussion of the relative significance of the m.s.o.f. is taken up in a later section of the paper.

Finite element formulation

Representation of local buckling fields. The local buckling fields are taken in the form

$$\{\boldsymbol{u}\} = \{\boldsymbol{u}^{(21)}\}\xi_i\phi_i(x) + \{\boldsymbol{u}^{(22)}\}\xi_i\xi_j\phi_i(x)\phi_j(x) \tag{26}$$

where ξ stands for the local buckling degrees of freedom, ϕ are the "slowing varying functions" which provide for amplitude modulation.

Choice of shape functions. A *p*-version finite element approach is adopted. A set of hierarchical polynomial functions are selected. For a sufficiently high "*p*" (polynomial degree), the problems of shear and membrane locking associated with lower order elements becomes inconsequential. A relatively small number of elements (in comparison to the *h*-version approach) would be sufficient resulting in considerable savings of effort in data input. The type of polynomials ϕ_i chosen in the present work are integrals of the Legendre functions, advocated by Szabo and Babuska (1991). These have been successfully used in postbuckling studies by Sridharan *et al.* (1992), and Kasagi and Sridharan (1992, 1993).

A cylindrical shell element based on Donnell's theory admitting shear deformation via the Reissner–Mindlin theory [eqn (3a–h)] is employed. The displacement functions take the form

$$\{\boldsymbol{u}\}^{\mathrm{T}} = \{u_{ij}\ v_{ij}\ w_{ij}\ \alpha_{ij}\ \beta_{ij}\}^{\mathrm{T}}\phi_i(x)\psi_j(y). \tag{27}$$

Note a similar, but one-dimensional, formulation has already been employed for the local buckling analysis (Sridharan *et al.*, 1992).

Strain–displacement matrix. As a first step in the formulation we set the *B*-matrix which relates the incremental strains to the incremental degrees of freedom. To this end, each strain component is expressed in terms of displacement variables of the local and overall fields. Thus, typically, the mid-plane strain ε_x (exclusive of mixed second order contributions) takes the form:

$$\varepsilon_x = u_{ik}\phi_i'\psi_k + \tfrac{1}{2}w_{ik}w_{jl}\phi_i'\phi_j'\psi_k\psi_l + \varepsilon_x^{(2)}\xi_i\phi_i + \varepsilon_x^{(22)}\xi_i\xi_j\phi_i\phi_j + \cdots \tag{28}$$

where:

$$\varepsilon_x^{(2)} = u_i^{(2)}\psi_i(y)\alpha_m \cos(\alpha_m x)$$

$$\varepsilon_x^{(22)} = \frac{\alpha_m^2}{4} w_i^{(2)} w_j^{(2)} \psi_i \psi_j + \left\{ 2\alpha_m u_i^{(22)} \psi_i + \frac{\alpha_m^2}{4} (w_i^{(2)} w_j^{(2)} + v_i^{(2)} v_j^{(2)}) \psi_i \psi_j \right\} \cos(2\alpha_m x) \tag{29}$$

where $\alpha_m = m\pi/L$, and a prime denotes differentiation w.r.t. x.

Equation (28) does not include the effects of m.s.o.f.s. This contribution (ε_x^*) is made up of two parts, namely $L_{11}(u^{(2)}, u^{(1)})$ and $L_1(u^{12})$ and their total contribution is neglected herein. This is discussed further in the next section, where a parameter is identified which if sufficiently small, the neglection may be justified.

Expressions similar to eqn (28) are written down for all the strain components. The incremental strain vector

$$\{\Delta\varepsilon\} = \{\Delta\varepsilon_x \ \Delta\varepsilon_y \ \Delta\gamma_{xy} \ \Delta\chi_x \ \Delta\chi_y \ \Delta\chi_{xy} \ \Delta\gamma_{xz} \ \Delta\gamma_{yz}\}$$

can be related to the incremental degrees of freedom. This relationship is expressed in terms of B-matrices as below:

$$\{\Delta\varepsilon\} = \left[[B_0] + \sum_{i=1}^{2} \{[B_i^c] \cos(i\alpha_m x) + [B_i^s] \sin(i\alpha_m x)\} \right] \{q\} \tag{30}$$

where q is the vector of incremental d.o.f.s arranged in any convenient order.

Current stresses $\{\sigma\}$ too are arranged in a similar form:

$$\{\sigma\} = \{\sigma_0\} + \sum_{i=1}^{2} [\{\sigma_i^c\} \cos(i\alpha_m x) + \{\sigma_i^s\} \sin(i\alpha_m x)] \tag{31}$$

and these must be available for every integration point on the surface of the structure.

The nonlinear analysis from this point on is standard and well documented (Zienkewicz, 1977). The tangential stiffness matrix $[K]$ is obtained as:

$$[K] = \int_A \left\{ [B_0]^T [H][B_0] + \frac{1}{2} \left[\sum_{m=1}^{2} [B_m^c]^T [H][B_m^c] + [B_m^s]^T [H][B_m^s] \right] \right\} dx\, dy \tag{32}$$

where the concept of slowly varying function of the overall and modulating function is employed. The vector of unbalanced forces at any stage in the analysis are given by:

$$\{\mathbf{f}\} = \{f_{ext}\} - \int_A [B]^T [\sigma]\, dx\, dy \tag{33}$$

where f_{ext} is the externally applied force. An arc length scheme (Crisfield, 1981) is used in tracing the nonlinear load deflection relationship. Initial imperfections are used to define the initial geometry corresponding to zero stress.

Relative significance of the mixed second order field (m.s.o.f.)

The inclusion of the m.s.o.f. in the present formulation, though entirely feasible does make it more complex. Fortunately, the influence of this field appears to be marginal in most cases. This was found to be true in earlier investigations of plate structures (Sridharan and Peng, 1989). Here we identify a parameter which acts as an index of the relative importance of the m.s.o.f.

Interactive buckling problem can be studied using a two d.o.f. model in the spirit of numerous earlier investigations [see, for example, Benito and Sridharan (1985)]. Consider a simplified potential energy function of a perfect stiffened structure undergoing interactive buckling written in terms of the dimensionless scaling parameters of the local and overall

modes of buckling (these take values of unity when the corresponding amplitude reaches a value equal to the shell thickness):

$$\Pi = (a_1 - \lambda b_1)\xi_1^2 + (a_2 - \lambda b_2)\xi_2^2 + c_1\xi_1^3 + d_1\xi_1^4 + d_2\xi_2^4 + c_{122}\xi_1\xi_2^2 + (d_{12} + d_{12}^*)\xi_1^2\xi_2^2. \quad (34)$$

The coefficients of the quadratic terms $a_1, \ldots, b_2$ are available from the linear stability analysis [cf. eqn (8)]. The cubic term in ξ_2 vanishes, as $m \gg 1$. The cubic term associated with the overall mode and the quartic terms associated with the individual modes are also readily set up. These take the form

$$\begin{aligned} c_1 &= H_{ij} L_{1_{ik}}(u_k^{(1)}) \cdot L_{2_{jl}}(u_l^{(1)}) \\ d_1 &= \Pi^{(11)} + \tfrac{1}{4} H_{ij} L_{2_{ik}}(u_k^{(1)}) \cdot L_{2_{jl}}(u_l^{(1)}) \end{aligned} \quad (35)$$

and a companion expression for d_2. Note that $\Pi^{(11)}$ takes the form similar to that of $\Pi^{(22)}$ given in eqn (10).

We, however, focus attention on the c_{122} and d_{12} terms arising from the interaction and these are given below:

$$\begin{aligned} c_{122} &= H_{ij} L_{1_{ik}}(u_k^{(1)}) \cdot L_{2_{jl}}(u_l^{(2)}) \\ \bar{d}_{12} &= \tfrac{1}{2} H_{ij} \{ L_{1_{ik}}(u_k^{(11)}) \cdot L_{2_{jl}}(u_l^{(2)}) + L_{1_{ik}}(u_k^{(22)}) \cdot L_2(u_l^{(1)}) + \tfrac{1}{4} L_{2_{ik}}(u_k^{(1)}) \cdot L_{2_{jl}}(u_l^{(2)}) \} \\ d_{12}^* &= \Pi^{(12)} + H_{ij} L_{11_i}(u_k^{(1)}, u_k^{(2)}) \cdot L_{11_j}(u_l^{(1)}, u_l^{(2)}). \end{aligned} \quad (36)$$

While the calculation of c_{122} and $\bar{d}_{12}$ involve only the two buckling modes and the second order fields associated with the individual modes, the d_{12}^* term depends upon the m.s.o.f. It is presumed here that the m.s.o.f. is evaluated imposing the orthogonality conditions [eqn (25)] and no higher local modes triggered in the interaction.

In the cases of stiffened structures which have no semblance of symmetry (such as stiffened plates or shells carrying stocky stiffeners), the cubic term associated with interaction (c_{122}) does not vanish and tends to dominate over the quartic terms in the determination of the maximum load-carrying capacity. d_{12}^* is the energy contribution of the mixed second order strains and stresses. It consists of two terms; the first term involves the m.s.o.f. displacements while the second term involves strains (and stresses) which arise purely by the interaction of the two buckling modes. The latter is positive, being the result of stresses working over strains of similar nature. The former may be viewed as a reaction of the structure which relaxes the strain energy associated with the latter and is invariably negative. Thus, these two effects tend to cancel each other, leaving a relatively small value for d_{12}^*. The ratio d_{12}^*/c_{122} may be viewed as an index of the relative influence of the m.s.o.f. contributions. As long as it is a small fraction, their influence is negligible. For a quantitative assessment, one may use the simplified model to determine the maximum load carried by the structure in the presence of imperfections in typical configurations of shell structures. This point is studied in some detail elsewhere (Sridharan, 1994) where it is shown that the inclusion of the field does not make an appreciable difference, and included as a "slave field" any improvement in accuracy claimed is questionable. Thus one may altogether neglect the mixed second order quantities, thus rendering the formulation considerably simpler. This is the approach taken here.

NUMERICAL STUDIES AND DISCUSSION

Performance of p-*version shell theory element*

The chosen shell element has an obvious lacuna in that it cannot model rigid body displacements. Notwithstanding this handicap, the element was found to perform very well in the moderately nonlinear range up to the limit point and in the earlier phase of load

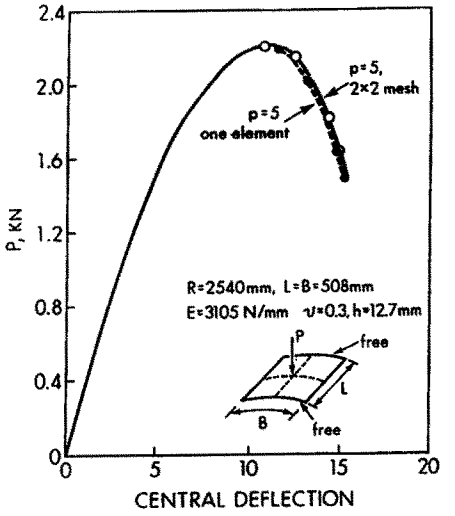

Fig. 3. Performance of p-version shell element.

shedding in several test cases. Its effectiveness increases with the p-level. The main advantage is its simplicity from the points of view of formulation and computation. Computational costs, however, escalate rapidly as the p-level is increased. Several bench mark problems were studied to examine the performance of the element. Element performed very satisfactorily for plate problems. As a test case, a clamped plate subjected uniform pressure was studied. It is seen that a single element with $p = 5$ produces a more accurate solution than 2×2 mesh of Heterosis elements, and 2×2 mesh with $p = 5$ does as well as sixteen four-node UI elements employed by Hughes and Liu (1981). It is only in shell problems that one must anticipate inaccuracies.

Figure 3 shows a shallow cylindrical shell hinged along one pair of opposite edges and free along the other pair. The shell carries a central concentrated load. The results are shown up to and beyond the limit point to include part of the unloading phase of the shell. These were obtained using, respectively, a single element for a quarter of the shell and 2×2 mesh with $p = 5$ in both cases. The results compare well with those obtained by Crisfield (1981). In the advanced post-limit state, the results of the present model deteriorate noticeably, but this is not considered significant in the present investigation where attention is confined to the initial postbuckling behavior.

Tvergaard panels: comparison with ABAQUS program

In this section we present a small number of results for the panels of infinitely wide stiffened plates studied by Tvergaard (1973). The geometry is illustrated in Fig. 4 and the accompanying Table 1 gives the details of the geometry of the two panels investigated. Note that h_0 represents the averaged ("smeared") thickness of the plate. The stiffeners are made sufficiently stocky so as to preclude the possibility of "stiffener buckling". The panels

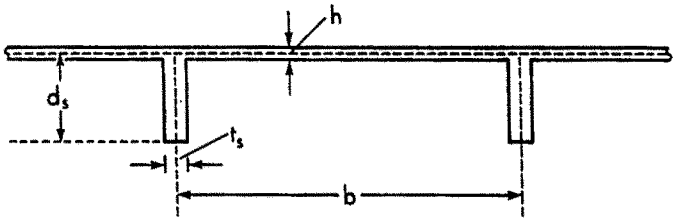

Fig. 4. Tvergaard type stiffened plate panel.

Table 1. Geometric parameters of Tvergaard panels ($L = 454.4$, $h_0 = 1.4544$)

Panel No.	L/b	d_s/b	h/h_0	m	$\sigma_1/E \times 10^3$	$\sigma_2/E \times 10^3$	σ_2/σ_1
1	4.0	0.10	0.688	6	0.469	0.471	1.004
2	8.0	0.20	0.410	11	0.683	0.697	1.020

are so designed that the local and overall critical stresses are given by the classical plate theory (CPT) under axial compression are the same and investigated extensively by Tvergaard (1973). The two panels considered were analysed with the following sets of imperfections:

$$\text{type 1}: \quad \bar{\xi}_1 = 0.1; \quad \bar{\xi}_2 = 0.1$$
$$\text{type 2}: \quad \bar{\xi}_1 = 0.0; \quad \bar{\xi}_2 = 0.2,$$

$\bar{\xi}_1$, $\bar{\xi}_2$ are, respectively, the actual imperfections in the overall and local modes, respectively ξ_1^0, ξ_2^0 divided by h_0. Only one half of the plate in the longitudinal direction is studied, thus taking advantage of symmetry. The calculations were performed with three elements, stiffener being represented by one element and each half of the panel on either side of the stiffener being modelled by a single element (Fig. 4). Noting that the element shape functions are used to capture only the overall action, the p-levels in the longitudinal and transverse direction were both chosen to be five. This guaranteed the elimination of shear-locking (Sridharan *et al.*, 1992) and full integration was adopted in numerical calculations. Boundary conditions were the same as in Tvergaard's analysis. The plate elements at the end boundaries of the structure were free to move in their own plane both longitudinally and transversely, but were restrained from out of plane deflections. The centerlines of panels (between the stiffeners) were given freedom to move in the plane of the plate but constrained to remain straight. Further symmetry conditions with respect to out of plane action ($\beta = 0$) were imposed along these lines. Initial imperfections in the form of local and overall buckling modes as obtained from a finite-strip analysis (Sridharan *et al.*, 1992) were introduced as initial values of the degrees of freedom.

The relationships between the axial stress carried and the maximum deflections (the local and overall contributions combined) at the center (between the stiffeners) are plotted for the two panels for the two cases of imperfections. These results are compared with those obtained using ABAQUS—a nonlinear finite element analysis program. Nine-noded Lagrangian isoparametric elements with reduced integration were used. The same discretization scheme was adopted for the two half panels on either side of the stiffener as well as the stiffener itself. Each of these substructures were divided into two elements transversely. The number of elements in the x-direction was dictated by the number of half-waves of buckling; one half of panel 1 (with $m = 6$) and panel 2 ($m = 11$) were covered by 12 and 24 elements, respectively. Subsequent computations with more refined meshes indicated that the error in the maximum capacity as given by these meshes was less than 0.5%.

Figure 5(a–d) gives the relationships between the axial stress and the maximum deflection at the central section of the panel for the four cases, as given by the present model and the ABAQUS program. The agreement between the maximum capacities of the panels are given by the present model and ABAQUS program is very close indeed in all the cases. The most noticeable discrepancies arise in the case of panel 1 where the error is of the order of 1–2% of the critical load. Even this from a practical stand point should be considered satisfactory. Comparing next the variation of the maximum deflection, the agreement is once again very close for panel 2. In the case of panel 1, some discrepancies are noticed throughout the loading history. This is attributable to two competing factors: (i) ABAQUS program captures the effects of several local modes, in particular those which are symmetric with respect to the stiffener, in contrast to the present model which is restricted to a single local mode; this effect is more significant for panel 1, which has greater stiffener spacing; (ii) the effects of mixed second order field contributions are completely neglected in the present model and these are seen to be slightly stabilizing in character as seen from the positive value of the coefficient d_{12}^* of the two parameter model. This effect becomes noticeable in the highly nonlinear range of the panel behavior causing a slight reduction in the stiffness in comparison to the ABAQUS model. In any case the present simpler model provides a good description of the behavior, adequate for preliminary and intermediate stages of design.

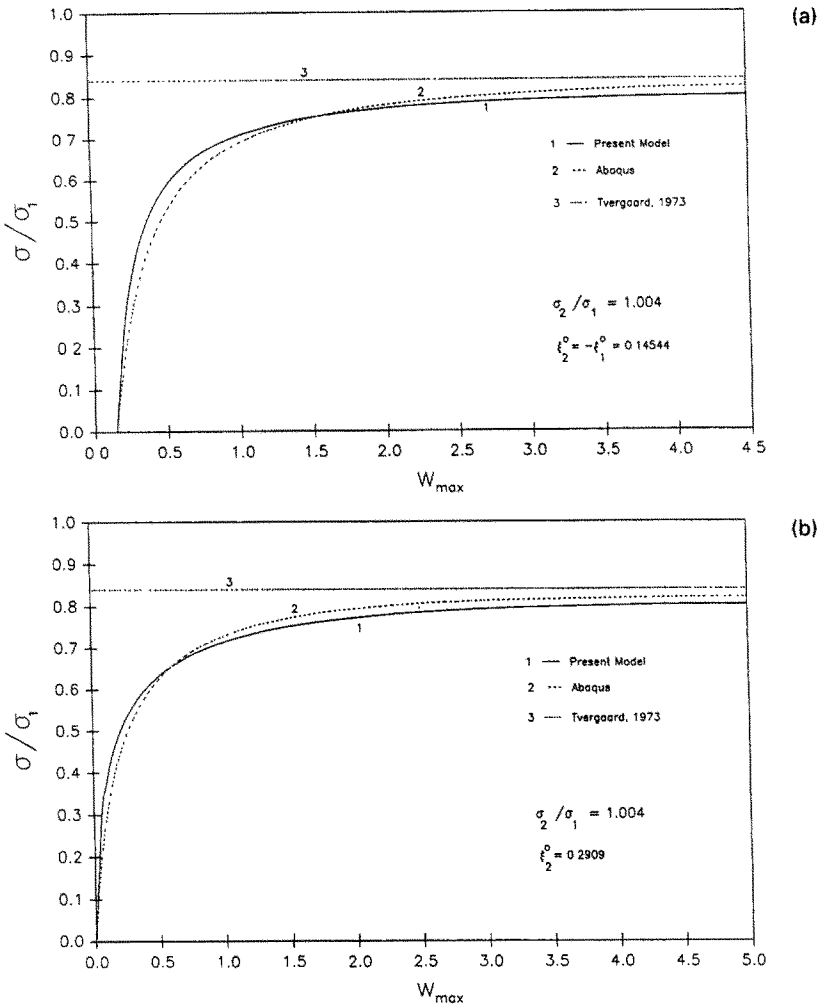

Fig. 5. Nondimensional axial stress vs maximum central deflection for (a) panel (1) and imperfection type (i); (b) panel (1) and imperfection type (ii); (c) panel (2) and imperfection type (i); (d) panel (2) and imperfection type (ii).

Figure 5(a–d) also indicate the load-carrying capacities as predicted by Tvergaard (1973). Whereas for the case of panel 2, Tvergaard's prediction of the maximum load is in complete agreement with those of the other two analyses, it overestimates slightly the load-carrying capacity in the case of panel 1. Tvergaard's analysis is very detailed, but does not account for amplitude modulation which plays the part of precipitating the limit point somewhat earlier.

Comparison with experimental results of Thompson et al.

Thompson *et al.* (1976) tested a series of small-scale specimens of integrally stiffened plates fabricated from epoxy plastic, a material which remains linearly elastic over a considerable range of strain. Initial imperfections in the local and overall modes by specified amounts were induced by causing permanent deformation at elevated temperatures. Two categories of stiffened plates were tested, one with stocky stiffeners and the other with slender stiffeners. In this section, we consider the former category of stiffened plates only and restrict ourselves to a case of near coincident critical stresses. These plates had eight bays with nine longitudinal stiffeners. The dimensions are as follows:

$$h = 0.75\,\text{mm}, \quad b = 57.7\,\text{mm}, \quad d_s = 9.625\,\text{mm}, \quad t_s = 4.90\,\text{mm}.$$

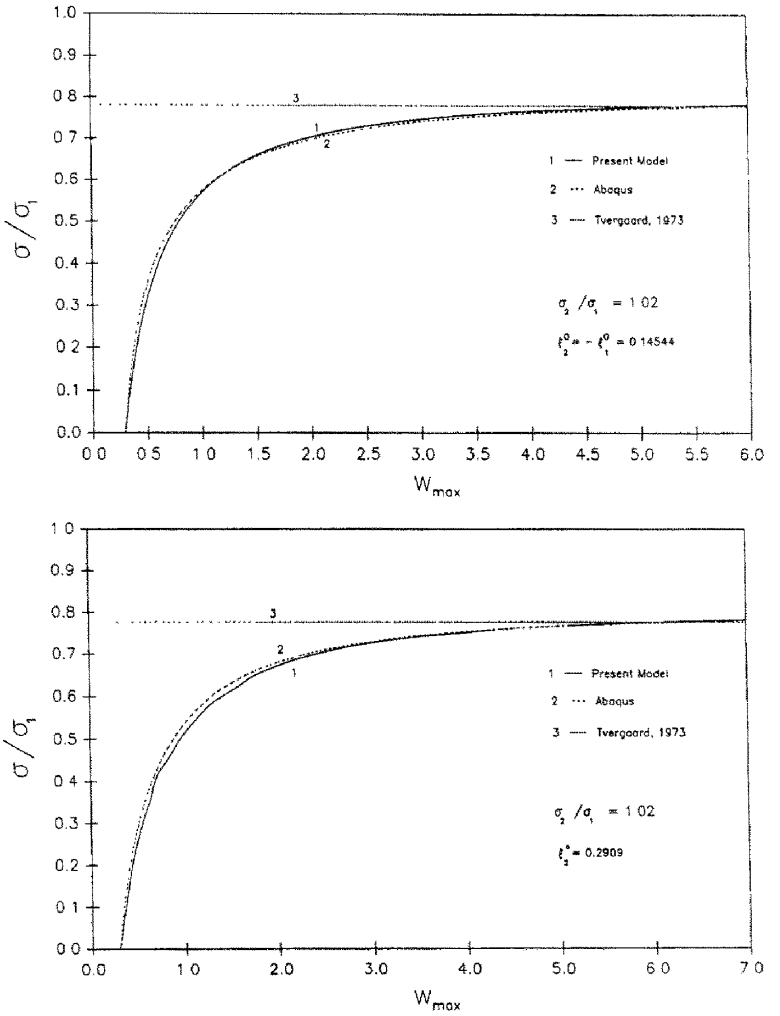

Fig. 5. *Continued.*

Thompson *et al.* take the local critical load in the form:

$$P_L = \frac{AkE\pi^2 h^2}{12(1-\nu^2)b^2}$$

where A is the total cross-sectional area of the plate and k is the buckling coefficient, taken as 6.96 in this case. Given further the ratio of P_L and P_E (the Euler critical load) as 1.02, the length L of the plate could be inferred as 307 mm. In the present study, all the analyses were performed using a typical panel and imposing symmetry conditions as in the previous section. Figure 6 shows the maximum stress carried by the panel (rendered dimensionless

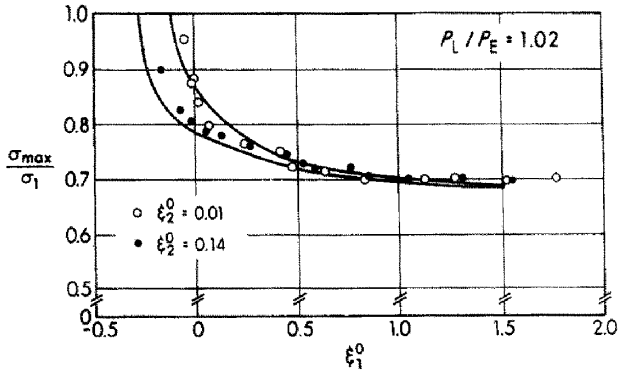

Fig. 6. Comparison with experimental results of Thompson *et al.* (1976).

by dividing it by the Euler critical stress of the isolated panel) for various values of overall imperfections for two sets of local imperfections. The agreement is generally satisfactory. For larger overall imperfections $\xi_1^0 > 1.0$, the theoretical results fall below the experimental values. This is due to the m.s.o.f. contributions neglected in the analysis. The latter, as seen from the value of d_{12}^*, have a small stabilizing effect for the panel. However the error is too small to be of concern.

From the foregoing comparisons, it appears that the assumptions made in the development of the model and, in particular, the neglection of the m.s.o.f. quantities are justified.

Cylindrical shell with five bays

Figure 7 shows a five-bay cylindrical shell structure carrying six longitudinal stiffeners. The geometry of the cross-section is given by:

$$b = 40t, \quad h = 0.5t, \quad d_s = 10t, \quad t_s = 2t, \quad R = 400t.$$

Two types of materials were considered, namely isotropic ($\nu = 0.3$) and composite with specially orthotropic properties. In the latter case the shell was deemed to be fabricated out of cross-ply laminate with a lay-up sequence of $\{0/90/0/90\}_s$ (0° orientation is the axial direction). The lamina material properties are given by

$$\frac{E_1}{E_2} = 18.28; \quad \frac{E_1}{G_{12}} = 37.39; \quad \nu_{12} = 0.24; \quad G_{12} = G_{23} = G_{31}$$

(cf. graphite/epoxy with $E_1 = 32{,}900$ ksi; $E_2 = 1{,}800$ ksi; $G_{12} = 880$ ksi).

The shells were assumed to be simply supported (in the "classical" sense, i.e. $w = v = \beta = 0$, $N_x = N_x^0$) at the ends. In addition they were restrained from radial deflection along the outer stiffener junctions. The stiffeners along the longitudinal edges were introduced to avoid local modes localized near these edges. The overall mode consisted of a single lobe across the section. The length of the structure in each case was chosen so as to make the local and overall critical stresses almost the same. Thus in the case of isotropic material, $L = 450t$ and $m = 18$ and for the composite material, $L = 495t$ and $m = 15$. The ratios of local to overall critical stresses were 1.015 and 1.000 in the isotropic and composite case, respectively. Note under prescribed uniform compression these shells exhibit stable post-local buckling behavior in the absence of the interaction with overall buckling.

The computations were carried out with eight elements taking $p = 5$ in both the longitudinal and transverse directions, with each stiffener represented by one element and the bays modelled with two elements each. Only one quarter of the structure is analysed in view of the symmetry. The responses of shells under axial compression were studied under

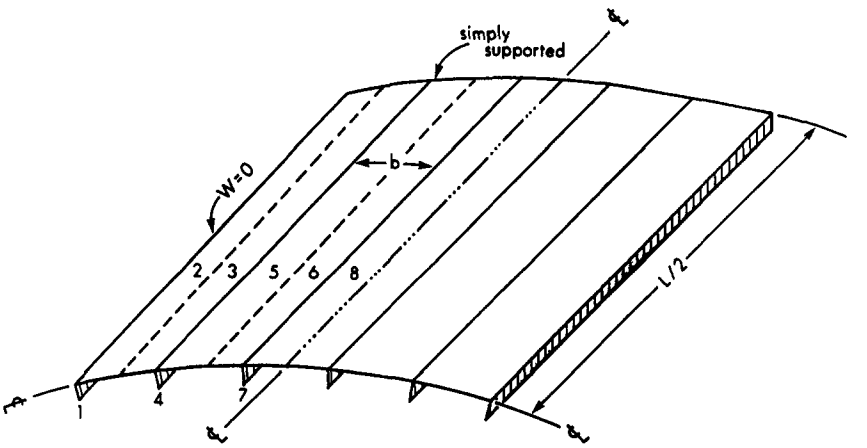

Fig. 7. Five-bay stiffened cylindrical shell.

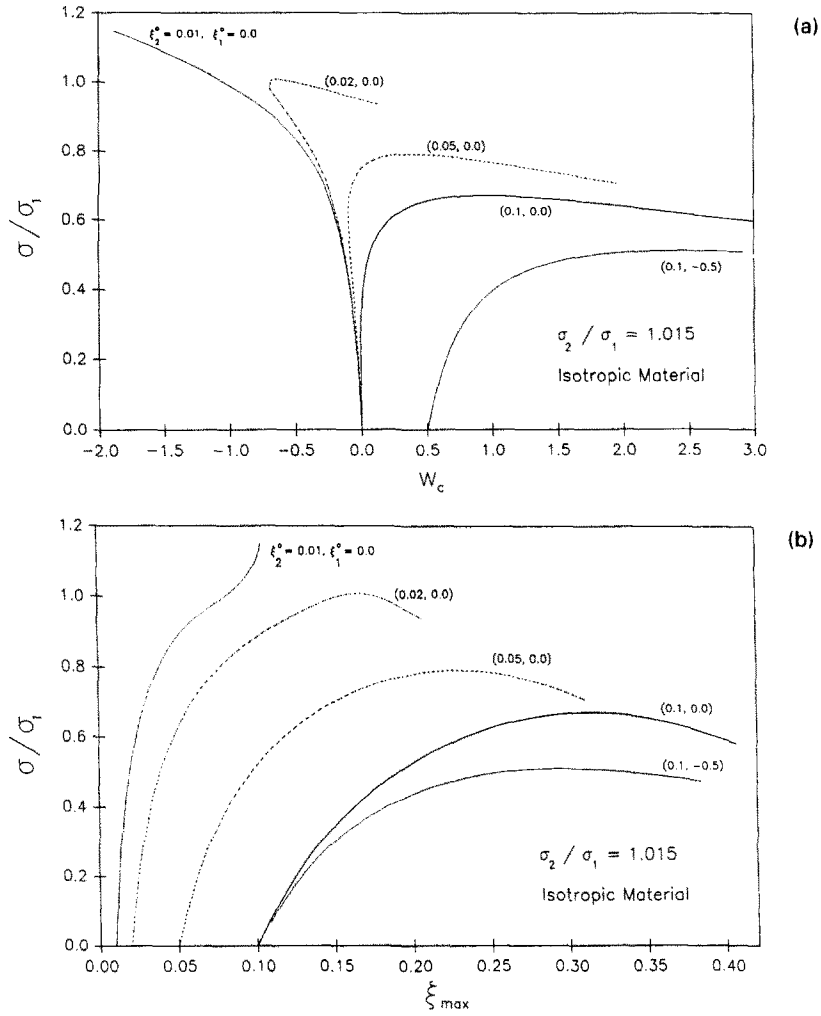

Fig. 8(a). Variation of maximum overall deflection with nondimensional axial stress for isotropic stiffened shell; (b) variation of maximum local buckling amplitude with nondimensional axial stress for isotropic stiffened shell.

a spectrum of initial imperfections. Some key results are given in Figs 8(a, b) and 9(a, b) for isotropic and composite shells, respectively.

Consider first the load-deflection response of the isotropic shell. The load is represented by the ratio of the applied stress to the overall critical stress. Figures 8(a, b) plot the variations, respectively, of the deflection at the center of the shell (W_c/t) and the maximum local buckling amplitude (ξ_{max}/t) with the nondimensional load for a variety of imperfections. (For simplicity, t is set to unity, i.e. $t = 1$, in further discussion.) In all except one case, the overall imperfections were taken to be zero and local imperfections of magnitudes 0.01, 0.02, 0.05 and 0.1 are considered. Finally, a case of combined local and overall imperfection is studied with $\xi_1^0/t = -0.5$, and $\xi_2^0/t = 0.1$.

It is observed that in the absence of significant imperfections, the shell under axial compression tends to bend outward in the prebuckling state and this continued outward bending causes the shell to buckle outward as the overall critical stress is approached. The bifurcation is of the "asymmetric" type leading to the stabilization of the structure. This is because the shell is thrown into a state of tension and the stiffeners are under compression due to the overall buckling. The stiffeners, being sufficiently stocky, are invulnerable to the additional compression. As the imperfections are increased the destabilizing cubic term $\xi_2^2\xi_1$ becomes important and reverses this tendency causing the shell to buckle inward. Severe imperfection-sensitivity is then observed, the shell losing 50% of its buckling strength under the same level of combined imperfections of the type that may be unavoidable in practice.

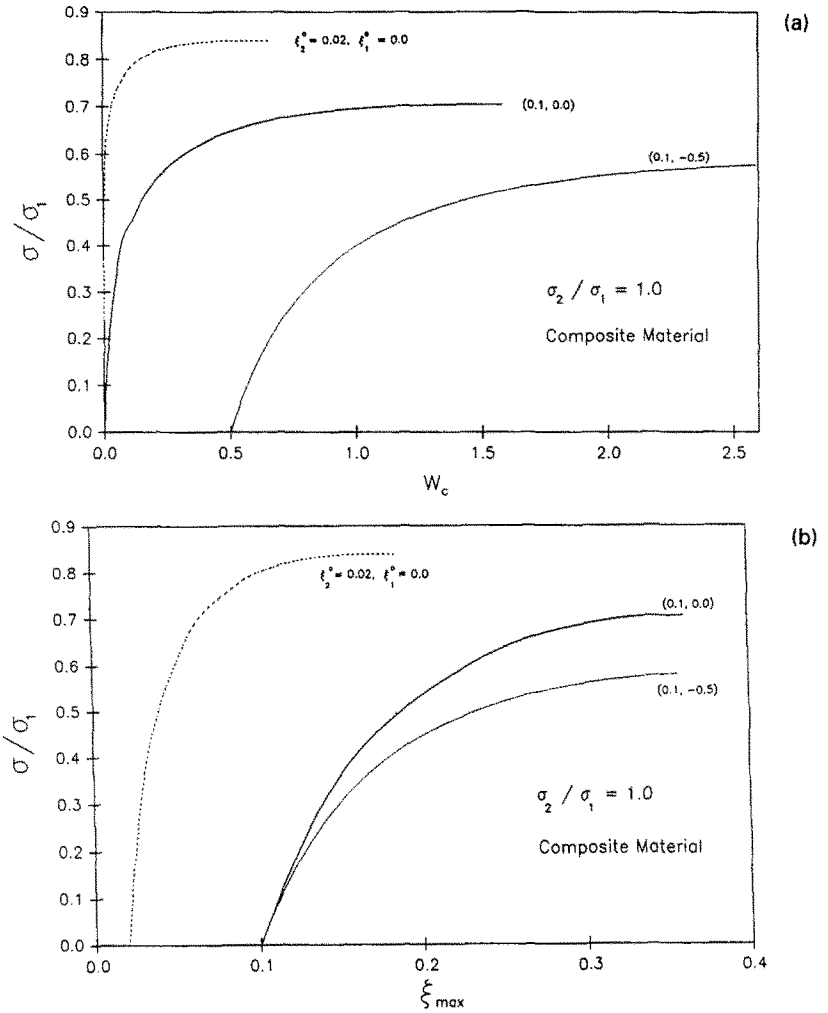

Fig. 9(a). Variation of maximum overall deflection with nondimensional axial stress for composite stiffened shell; (b) variation of maximum local buckling amplitude with nondimensional axial stress for composite stiffened shell.

Figure 9(a, b) plots the response of the composite shell for three levels of imperfections. The response is similar to that of the isotropic case, though the outward bending tendency in the early stages of loading is less marked. Imperfection-sensitivity too is slightly less, the erosion of load-carrying capacity being about 44% of the critical load under combined imperfections.

CONCLUSIONS

A novel approach to the solution of the problems of interaction of local and overall instabilities in stiffened plate and shell structures has been presented. Axially compressed stringer-stiffened plates and shells were considered in particular. The essential concept involved is the embedding of the local buckling deformation together with the associated second order effects in a shell element. The growth of local buckling deformations is controlled by a small number of additional degrees of freedom associated with the element and these also allow for amplitude modulation.

The development of the new model was simplified by neglecting the contributions of the mixed second order field displacements, strains and stresses. This assumption was argued at some length, but the final justification rested upon the excellent agreement between the predictions of the present model and those of full-blown nonlinear analyses. Comparisons with experimental results also confirm the accuracy of the present model.

Stringer-stiffened cylindrical shells under axial compression and near coincident buckling were found to be vulnerable to modal interaction and can lose 50% of their buckling strength in the presence of imperfections of the type unavoidable in practice.

It is found that the new methodology offers a superior alternative to the full-blown nonlinear analysis. The number of degrees of freedom required are only marginally greater than those required for the overall bending/buckling analysis only, irrespective of the number of half-waves of local buckling.

Acknowledgement—Support for this research was provided in part by the NASA Langley Research Center under Grant No. NAG-1-1279.

REFERENCES

ABAQUS (1992). Version 5.2. Hibbit, Karlsson & Sorenson Inc., Newark, CA.

Ashraf Ali, M. A., and Sridharan, S. (1988). A versatile model for interactive buckling of columns and beam columns. *Int. J. Solids Structures* **24,** 481–496.

Benito, R. and Sridharan, S. (1985). Interactive buckling analysis with finite strips. *Int. J. Numer. Meth. Engng* **21,** 145–161.

Budiansky, B. (1966). Dynamic buckling of elastic structures: criteria and estimates. In *Dynamic Stability of Structures* (Edited by G. Herrmann), pp. 83–106. Pergamon Press, New York.

Bushnell, D. (1985). *Computerized Buckling Analysis of Shells.* Martinus Nijhoff, Dordrecht, The Netherlands.

Byskov, E. and Hutchinson, J. W. (1977). Mode interaction in axially stiffened cylindrical shells. *AIAA J.* **15**(7), 941–940.

Crisfield, M. A. (1981). A fast incremental/iterative solution procedure that handles snap-through. *Comput. Structures* **13,** 55–62.

Hughes, T. J. R., and Liu, W. K. (1981). Nonlinear finite element analysis of shells: part I, three dimensional shells. *Comput. Meth. Appl. Mech. Engng* **26,** 331–362.

Kasagi, A. and Sridharan, S. (1992). Postbuckling analysis of layered composites using p-version finite strips. *Int. J. Numer. Meth. Engng* **33**(10), 2091–2107.

Kasagi, A. and Sridharan, S. (1993). Buckling and postbuckling analysis of thick composite cylindrical shells under hydrostatic pressure. *Compos. Engng* **3**(5), 467–487.

Koiter, W. T. and Pignataro, M. (1976a). An alternative approach to the interaction of local and overall buckling in stiffened panels. In *Buckling of Structures* (Edited by B. Budiansky), pp. 133–148. Springer-Verlag, New York.

Koiter, W. T. and Pignataro, M. (1976b). *A General Theory of Mode Interaction in Stiffened Plate and Shell Structures.* Report 590. Laboratory of Engineering Mechanics, Delft Institute of Technology, The Netherlands.

Sridharan, S. and Peng, M.-H. (1989). Performance of stiffened panels. *Int. J. Solids Structures* **25**(8), 879–899.

Sridharan, S., Zeggane, M. and Starnes, J. H. (1992). Postbuckling response of stiffened composite cylindrical shells. *AIAA J.* **30**(12), 2897–2905.

Sridharan, S. (1994). *The Scope and Limitations of Two Parameter Models in Interactive Buckling Analysis.* Report 93. Department of Civil Engineering, Washington University in St. Louis.

Szabo, B. A. and Babuska, I. (1991). *Finite Element Analysis*, pp. 95–117. Wiley, New York.

Thompson, J. M. T., Tulk, J. D. and Walker, A. C. (1976). An experimental study of imperfection-sensitivity in interactive buckling of stiffened plates. In *Buckling of Structures* (Edited by B. Budiansky). Springer-Verlag, New York.

Tvergaard, V. (1973). Influence of postbuckling behavior in optimum design of stiffened panels. *Int. J. Solids Structures* **9,** 1519–1534.

Zienkiewicz, O. C. (1977). *The Finite Element Method.* McGraw-Hill, London.